Cancer Chemother Pharmacol (2002) 49: 57–68
DOI 10.1007/s00280-001-0385-3

ORIGINAL ARTICLE

Daniel E. Lopes de Menezes · Lawrence D. Mayer

Pharmacokinetics of Bcl-2 antisense oligonucleotide (G3139) combined with doxorubicin in SCID mice bearing human breast cancer solid tumor xenografts

Received: 1 May 2001 / Accepted: 31 August 2001 / Published online: 20 November 2001

Abstract *Purpose*: To evaluate the pharmacokinetic (PK) properties of Bcl-2 antisense oligodeoxynucleotide G3139 when combined with the anthracycline anticancer drug doxorubicin (DOX) in a model of MDA435/LCC6 human breast cancer in severely compromised immunodeficient (SCID) mice. *Methods*: An orthotopic model of MDA435/LCC6 solid breast tumors was developed by bilateral implantation of passaged cells in female SCID-RAG2 mice. The G3139 plasma profile was compared for two common routes of administration (i.v. or i.p.) in single and multiple dose treatment regimens of 5 mg/kg G3139 alone or with simultaneous DOX (5 mg/kg) administration. At selected times, plasma and major organs were assayed for [^{3}H]G3139 using scintillation counting and DOX determined using HPLC. The molecular integrity of G3139 was analyzed using SDS-PAGE. The PKs of G3139 and DOX were evaluated using a two-compartment model. *Results*: G3139 administered i.v. at 5 mg/kg revealed a biexponential plasma concentration-time curve with a Cmax of 99.9 μg/ml and elimination half-lives of 0.03 h and 9.8 h, respectively, which resulted in an area under the concentration-time curve (AUC) of 15.9 μg·h/ml. G3139 administered i.p. showed a plasma absorption, distribution and elimination profile typical of this route of administration, characterized by half-lives of 0.03 h, 0.2 h and 8.9 h, respectively and a Cmax of 8.6 μg/ml. Based on AUC comparisons, the bioavailability of G3139 injected i.p. was 84% compared to i.v. administration. Subtle changes were observed in G3139 PKs after three prior i.p. doses of G3139. Specifically, a sixfold slower absorption rate, lower Cmax (6.9 μg/ml), increased Tmax (0.2 h), and an AUC of 17.4 μg·h/ml were observed, consistent with concentrations approaching saturation levels in tissue sites to which G3139 distributes. Coadministration of DOX had significant effects on the PK properties of G3139, manifested by an increased Cmax (11.2 μg/ml), higher AUC (19.7 μg·h/ml), and ninefold lower plasma clearance for single-dose G3139 administration. G3139 in plasma remained largely intact (< 17% degraded in plasma over 4 h), and increased plasma protein association occurred as a function of time. G3139 was detected in both healthy and tumor tissue after i.v. and i.p. administration. The highest tissue levels of G3139 were observed in the kidneys (40 μg/g), and low levels (< 2 μg/g) were detected in lung, heart and muscle. The rate of accumulation of G3139 in organs was dependent upon G3139 levels in plasma and the presence of coadministered DOX. Significant accumulation of G3139 was observed in solid tumors, with peak levels of approximately 5 μg G3139/g tumor, and approximately a two- to threefold tumor/muscle AUC ratio. The kinetics of G3139 accumulation in tumor tissue increased with increasing circulating G3139 concentration. The tissue distribution properties of DOX were also altered in the presence of coadministered G3139: in the presence of G3139, tumor exposure to DOX increased two- to threefold without alteration in plasma DOX PKs. *Conclusions*: These findings indicate that drug-drug interactions between G3139 and DOX are modest and favorable in that elevated tumor DOX levels are achieved without compromising G3139 tumor uptake or significantly altering plasma drug concentrations.

Keywords Antisense · Bcl-2 · Doxorubicin · Pharmacokinetics · Breast cancer

D.E. Lopes de Menezes · L.D. Mayer (✉)
Department of Advanced Therapeutics,
B.C. Cancer Research Centre, 601 W 10th Ave.,
Vancouver, B.C. V5Z 4E6, Canada
E-mail: lmayer@bccancer.bc.ca
Tel.: +1-604-8776098
Fax: +1-604-8776011

L.D. Mayer
Faculty of Pharmaceutical Sciences,
2146 East Mall, University of British Columbia,
Vancouver, B.C. V6 T 1Z3, Canada

Present address: D.E. Lopes de Menezes
Pharmacology and Preclinical Affairs,
Chiron Corporation, 4560 Horton St.,
m/s T-200, Emeryville, CA 94608, USA

Abbreviations *AS:* antisense · *AUC:* area under the concentration-time curve · *Cmax:* maximum concentration · *CL:* clearance · *DOX:* doxorubicin · *i.p.:* intraperitoneal · *i.v.:* intravenous · *K01/K10:* respective absorption and elimination rate constants · *K01 half-life/K10 half-life:* respectively absorption and elimination half lives · *ODN:* oligonucleotide · *PK:* pharmacokinetics · *SCID:* severely combined immunodeficient · $t_{1/2}\alpha$*:* distribution half life · $t_{1/2}\beta$*:* elimination half life · *Tmax:* time to Cmax · *V:* volume of distribution

Introduction

Overexpression of the oncogene product Bcl-2 is associated with chemoresistance in a variety of cancers, the mechanism involving the inhibition of programmed cell death or apoptosis [1, 2, 3, 4]. Recently, antisense oligonucleotides (AS ODNs) to Bcl-2 have been developed as a novel strategy to modulate Bcl-2 levels in tumor cells via specifically hybridizing to complementary regions of the mRNA coding Bcl-2 [5]. Downregulation of Bcl-2 is believed to occur by direct AS ODN mRNA inhibition and/or degradation of these duplexes by RNAse H resulting in an inhibition of Bcl-2 protein translation [6, 7]. Specific properties of AS ODNs, i.e., ODN sequence, chemical modification of the ODN sequence, stability, RNA binding affinity, RNase H activity, and cellular uptake, determine the effectiveness of the ODN as a therapeutic agent [8].

Recently, a phosphorothioate AS sequence directed against the open reading frame of the Bcl-2 RNA (G3139; Genta, Berkeley Heights, N.J.) has been shown to be effective in a variety of tumor models in vitro and in vivo and is currently in clinical development [9, 10, 11]. Since many cytotoxic drugs are believed to act by inducing apoptosis, concurrent Bcl-2 AS ODN and drug treatment presents an effective strategy resulting from possible AS ODN-drug synergism [12, 13, 14, 15, 16, 17, 18]. Prior to combining AS ODNs with chemotherapeutics, understanding the in vivo PKs of each drug is imperative to identify potential drug interactions that may result in adverse or favorable biological responses. PK studies allow predictions of drug bioavailability, drug exposure to target tissues, and identification of organs of potential toxicity. Few studies have examined the PK properties and tumor delivery of G3139 [9, 19]. Furthermore, there are no published reports on the effects of multiple treatments or coadministered chemotherapeutics on the PK properties of G3139. Given the high DNA-binding avidity of certain anticancer drugs, such as doxorubicin (DOX), possibilities exist for DOX-G3139 interactions both in the circulation and in tissues, and these could affect the bioavailability of both agents.

In this study, we evaluated the PK properties of G3139 in MDA435/LCC6 breast cancer tumor-bearing SCID mice to define the PK properties of G3139 in the presence and absence of DOX, and in order to evaluate possible G3139-drug PK interactions and help elucidate the relationship between therapeutic responses and the concentrations of G3139 in plasma and solid tumors.

Materials and methods

AS ODN and drugs

The phosphorothioate ODN (18-mer), G3139, with a sequence complementary for the first six codons of the open reading frame of Bcl-2 mRNA (5′-tct ccc agc gtg cgc cat-3′, molecular weight 5684.58 Da) was used as the AS ODN, and was a gift from Genta (Berkeley Heights, N.J.). [^{3}H]G3139 was prepared by inserting a non-exchangeable [^{3}H] at the 5′ position of the thymidine of G3139 (Trilink Biotechnologies, San Diego, Calif.). Doxorubicin (DOX) was from Faulding (Vaudreuil, Quebec). Acetonitrile, acetone, propan-2-ol, and ammonium formate were of either analytical or HPLC grade.

Cell lines, mice and tumor models

The human breast cancer cell line MDA435/LCC6 was obtained from Dr. R. Clarke, Georgetown University [20]. Female SCID-RAG2 mice (4–6 weeks of age, 18–22 g) were obtained from the BC Cancer Agency Joint Animal Facility breeding colony and kept in an aseptic environment. MDA435/LCC6 cells were routinely maintained by serial passages of ascites i.p. in SCID-RAG2 mice. An orthotopic tumor model of MDA435/LCC6 cells in RAG2 mice was established by bilateral implantation of 2×10^6 in vivo-passaged MDA435/LCC6 cells into the mammary fat pad. All animal protocols were approved by the B.C. Cancer Agency Animal Welfare Committee.

PKs and tissue distribution

PK experiments with [^{3}H]G3139 were conducted in female RAG2 mice bearing MDA435/LCC6 tumors (0.1–0.15 g). The PKs of G3139 (5 mg/kg) were compared after a single bolus injection either i.v. or i.p.. In addition, the PK properties of G3139 (5 mg/kg) were examined after three consecutive i.p. doses given on days 1–4. The PKs of G3139 were also studied in the presence and absence of DOX (5 mg/kg) given i.v. 1 h before the G3139 injection. At selected times after G3139 treatment, mice (three per group) were euthanized by CO_2 asphyxiation over 6 h. Blood was collected via cardiac puncture and placed into EDTA-coated microtainer tubes. Plasma was isolated from whole blood by centrifugation at 500 *g* for 10 min. Major organs (i.e., liver, spleen, lung, heart, kidney), muscle and solid tumor were dissected, rinsed in PBS, dried, and weighed into glass tubes. A 20% homogenate of liver in distilled water was prepared using a Polytron homogenizer (Kinematica, Switzerland). [^{3}H]G3139 was determined in plasma and tumor/tissue homogenates using Solvable (Packard, Missasauga, Ont.), a tissue solubilizer, (50ºC overnight) and treatment with a cocktail of 200 m*M* EDTA, 30% H_2O_2 and 10 *N* HCl for 1 h at room temperature. The amount of radioactivity in samples was determined using scintillation counting (TRI-CARB Model 1900, Packard Instrumentation, Meridien, Ct.).

HPLC analysis of DOX

DOX in plasma and tissues was determined using a previously described HPLC method [21, 22]. Briefly, DOX was extracted from plasma or tissue homogenates with acetonitrile and reconstituted in mobile phase consisting of 16 m*M* ammonium formate (pH 3.5)/acetone/isopropanol (75:20:5). Samples were run using isocratic elution on a Waters 2690 HPLC with a built-in autosampler

(Milford, Mass.), a C18 guard column (Waters), a Nova-Pak C18 analytical column (Waters), and a Waters 474 fluorescent detector. The concentrations of DOX in various organs were determined from a previously prepared calibration curve utilizing background fluorescent corrections for drug-free organs and appropriate tissue/blood correction factors.

In vivo stability and plasma protein association of G3139 in plasma

The molecular weight characteristics of radioactive G3139 and plasma protein binding were determined using SDS-PAGE to determine the in vivo stability of G3139. SCID mice were injected with 5 mg/kg G3139 (containing [^{3}H]G3139) and blood was isolated at specific time-points (0.083, 0.5, and 4 h) after injection. ODNs were extracted from plasma using a modified procedure as previously described [23]. Briefly, plasma was incubated with proteinase K (1 mg/ml) in an extraction buffer of 0.5% SDS, 10 m*M* NaCl, 20 m*M* Tris-HCl, pH 7.6, 10 m*M* EDTA for 2 h at 37ºC. The samples were extracted twice with phenol/chloroform/isoamyl alcohol (25:24:1 v/v) and once with chloroform. Extracted ODNs were precipitated with 75% ethanol and reconstituted in distilled water. Both ODNs in plasma and extracted ODNs were then run on a 20% SDS-PAGE gel containing 7 *M* urea. Biorad standards were run to identify points on the gel of appropriate molecular weight. The gel was cut up and [^{3}H] levels determined using the Solvable procedure and scintillation counting (see PK methods).

PK modeling and statistical analyses

The plasma and tumor data were modeled using WinNonLin version 1.5 PK software (Pharsight Company, Mountain View, Calif.). One-, two-, and three-compartment models and first-order administration were tested for fit to the plasma and tumor data. Appropriate models to fit the plasma and tumor data were selected based on the goodness of fit for each model, including the visual assessment of the distribution of residuals, rank and Akaike's information criterion. Curves were appropriately weighted to accurately fit the absorption, distribution and elimination phases. All linear regression was done using Microsoft Excel (Seattle, Wash.). Student's *t*-test was used to determine the significance of differences between two treatment groups. Multiple comparisons were done using one-way analysis of variance (ANOVA), and post-tests comparing different treatment means were done using Bonferroni's test (Statistica release 4.5, StatSoft, Tulsa, Okla.). Differences were considered significant for *P*-values < 0.05.

Results

Comparison of single-dose i.v. versus i.p. PK of G3139

We first compared the PKs and biodistribution after a single i.v. bolus or i.p. injection of [^{3}H]G3139 (5 mg/kg) in MDA435/LCC6 tumor-bearing mice. G3139 administered i.v. revealed a biexponential plasma concentration-time curve (Fig. 1A), described by a two-compartment model with first-order elimination. The descriptive PK parameters are summarized in Table 1. The plasma concentration-time profile exhibited a Cmax of 99.9 μg/ml, and an AUC of 15.9 μg·h/ml (Table 1). The two distinct phases of the curve revealed a short distribution half-life of 0.03 h and longer terminal elimination half-life of 9.8 h (Table 1). This suggests that G3139 was distributed and eliminated rapidly, as seen from its high distribution rate constant K12 (10.1 h^{-1}) and plasma clearance (CL 10.5 ml/h). The kidneys showed the highest peak concentration of G3139 (40 μg/g tissue), suggesting that urinary excretion was the primary route of elimination. G3139 was also distributed to relatively high levels in liver and spleen (9–11 μg/g tissue) and to lower levels in lung, heart and muscle (< 5 μg/g tissue). The radioactivity persisted in various organs for up to 6 h, with a slow rate of G3139 turnover from the liver (Fig. 1). This was also reflected by the tissue distribution rate constants: the ratio K12/K21 was 2.7, indicating net transfer of G3139 to the peripheral compartment (K21 3.8 h^{-1} compared to K12 10.1 h^{-1}).

G3139 after i.p. injection showed characteristic absorption, distribution and elimination profiles associated with this route of administration. A single bolus i.p. dose of 5 mg/kg produced plasma and tissue distribution profiles described by a first-order two-compartment model with first-order absorption and elimination, following a short lag time (Fig. 1). Compared to G3139 given i.v., low plasma concentrations of G3139 were attained shortly after i.p. dosing (2.6 μg/ml at 0.08 h), as G3139 plasma levels were dependent upon the absorption of G3139 from the peritoneal cavity. Accumulation of G3139 in plasma after i.p. injection occurred with a relatively short absorption half-life (K01 half-life) of 0.03 h, a distribution half life of 0.2 h and an elimination half-life of 8.9 h. The Cmax was 8.6 μg/ml with a time to Cmax (Tmax) of approximately 0.2 h. The plasma AUC following i.p administration was slightly lower than that following i.v. administration (13.3 vs 15.9 μg·h/ml, $P < 0.05$) indicating a bioavailability of 84%.

After absorption, the distribution and elimination kinetics of G3139 administered i.p. were also different from those after i.v. administration, with $t_{1/2}\alpha$ and $t_{1/2}\beta$ of 0.2 and 8.9 h, respectively, possibly because of a continuous influx of G3139 from the i.p. depot. Distribution constants were strikingly different, and clearance was 3.3-fold lower after i.p. than after i.v. administration (3.2 vs 10.52 ml/h, Table 1). The organ distribution of G3139 was markedly different following i.v. and i.p. administration, except for the liver (Fig. 1). In all cases, G3139 distribution into organs following i.v. administration showed a sharp concentration spike, and in all cases was two- to tenfold higher than following i.p. administration.

PK properties of G3139 administered i.p. in multiple dosage regimens

Daily i.p. injections of G3139 have been shown to produce steady-state plasma levels after approximately 72 h [9]. To understand the PK properties of G3139 after repeated administration in the preclinical tumor

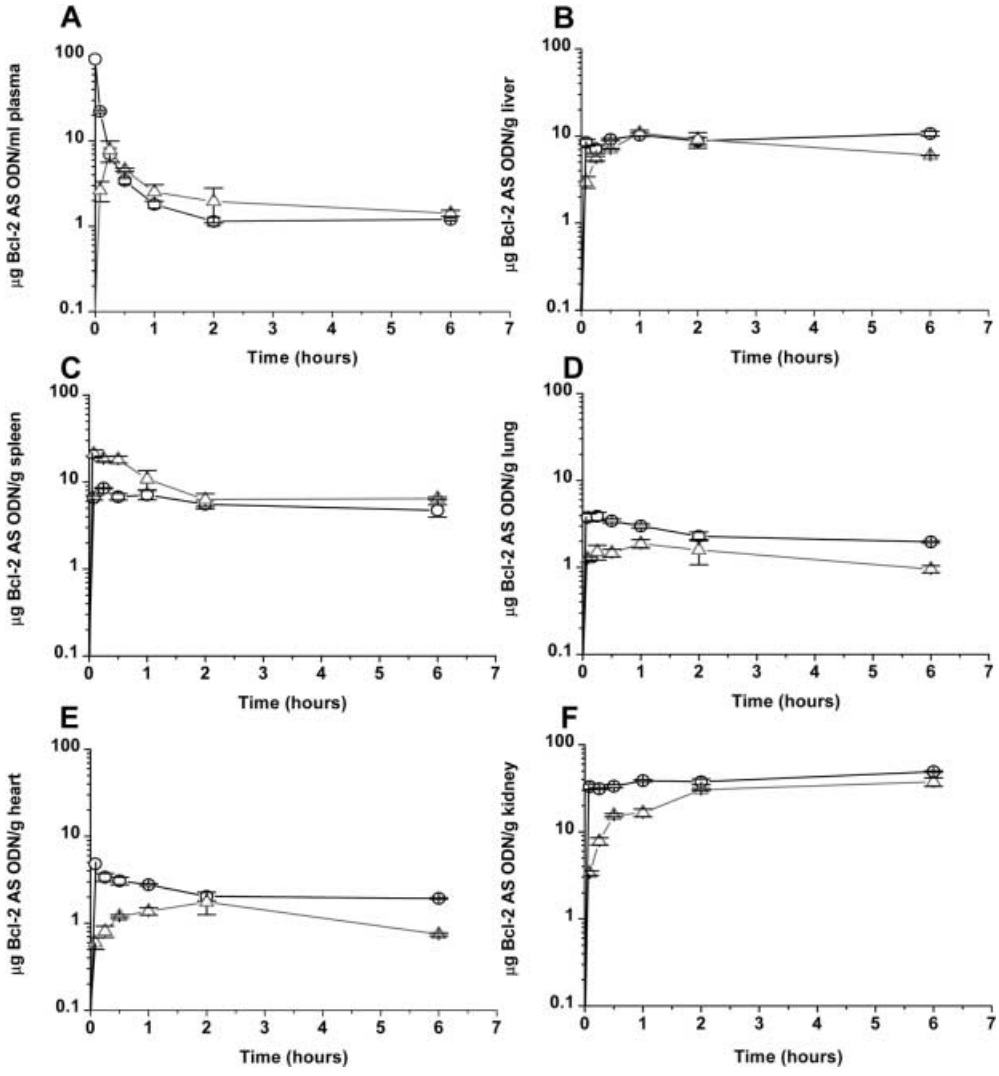

Fig. 1A–F Comparison of the concentration-time profiles of G3139 in plasma and various organs after a single i.v. or i.p. dose of G3139 to MDA435/LCC6 tumor-bearing SCID-RAG2 mice. Mice with tumors (0.1–0.15 g, day 17) were injected with a single bolus dose of [^{3}H]G3139 (5 mg/kg) either i.v. (*open circles*) or i.p. (*open triangles*). Levels of G3139 in plasma (**A**), liver (**B**), spleen (**C**), lung (**D**), heart (**E**), and kidney (**F**) were determined at the indicated times using scintillation counting for [^{3}H] (see Materials and methods). Data are expressed as means ± SD ($n = 3$ mice per time-point)

Table 1 Summary of selected pharmacokinetic (PK) parameters of G3139 and doxorubicin (DOX) in plasma after the indicated treatments. RAG2 mice bearing MDA435/LCC6 tumors were treated with a single i.v. or i.p. dose of 5 mg/kg of G3139 on day 17 after tumor implantation (0.1 g tumor weight). Mice were killed at selected times after [^{3}H]G3139 treatment and the amount of [^{3}H]G3139 in plasma determined using scintillation counting (see Methods). Data are means ($n = 3$ mice per time-point, 18 mice per treatment group). DOX was determined in plasma samples by HPLC. PK parameters were estimated using WinNonLin using a two-compartment model with first-order input and elimination (*Cmax* maximum concentration in plasma; $AUC_{0\text{-}t}$ area under the concentration-time curve; *V* volume of distribution; *K01*, *K10*, *K12*, *K21* absorption and distribution rate constants between compartments 1 and 2; $t_{1/2}\alpha$ distribution half life; $t_{1/2}\beta$ elimination half life; *CL* plasma clearance)

Drug	Route/ treatment	Cmax (μg/ml)	$AUC_{0\text{-}t}$ (μg·h/ml)	V (ml)	K01 half-life (h)	$t_{1/2}\alpha$ (h)	$t_{1/2}\beta$ (h)	K01 (h^{-1})	K10 (h^{-1})	K12 (h^{-1})	K21 (h^{-1})	CL (ml/h)
G3139	i.v.	99.9 ± 0.5	15.9 ± 0.6	3.6	–	0.03	9.8	–	10.51	10.06	3.80	10.52
	i.p.	8.6 ± 0.8	13.3 ± 1.1	8.8	0.03	0.20	8.9	24.6	0.34	2.43	0.74	3.2
	i.p. (after three prior i.p. doses)[a]	6.9 ± 1.9	17.4 ± 2.2	7.1	0.17	0.21	3.5	4.1	0.63	1.83	1.03	4.4
	i.p. (after three prior i.p. doses + DOX)[b]	11.2 ± 1.4	19.7 ± 2.0	7.7	0.04	0.78	209.7	19.7	0.05	0.78	0.06	0.4
DOX	i.v.	0.6 ± 0.05	3.0 ± 0.4	667	–	0.23	50.5	–	0.06	2.24	0.74	9.3
	i.v. (after three prior i.p. G3139 doses)[c]	0.4 ± 0.03	3.2 ± 0.3	592	–	0.30	37.4	–	0.04	1.24	1.04	11.1

[a]Mice were given 5 mg/kg of G3139 on days 17–19 and the G3139 PK determined on day 20
[b]Mice were given 5 mg/kg of G3139 on days 17–19 and the G3139 PK determined on day 20 in the presence of DOX (5 mg/kg given i.v. 1 h prior to G3139)
[c]Mice were given 5 mg/kg of G3139 on days 17–19 and the DOX PK determined on day 20

model investigated here, we injected the tumor-bearing mice with [^{3}H]G3139 i.p. after three daily doses of unlabeled G3139 at 5 mg/kg. Differences in the plasma PK parameters were observed between a single i.p. dose and an i.p. dose given after three prior doses (Fig. 2). Interestingly, the circulating G3139 levels from three prior doses had a dramatic effect on the absorption rate of G3139 from the i.p. cavity: there was a sixfold increase in the absorption half-life to 0.17 h, equivalent to a decrease in K01 to 4.1 h^{-1}. The mean Cmax attained was slightly lower but not significantly different (6.9 μg/ml for multiple doses vs 8.6 μg/ml for a single dose, $P > 0.05$) with a delay in Tmax from 0.2 to 0.4 h. Also, the AUC was marginally elevated (17.4 μg·h/ml after multiple doses vs 13.3 μg·h/ml after a single dose, $P < 0.05$) possibly as a result of a smaller volume of distribution, consistent with close to equilibrium levels of G3139 in plasma and tissue compartments (lower K12, K12≅K21; Table 1). Furthermore, tissue distribution profiles of G3139 appeared to reach near saturation in various organs, reflected by slower absorption, distribution and elimination profiles of the drug (Fig. 2).

In vivo stability and protein binding of G3139

To ensure that the PK properties of G3139 were those of the intact molecule and not those of degraded and/or dissociated [^{3}H]G3139 label, we confirmed the molecular weight identity of the ODN using SDS-PAGE. SCID mice were injected with [^{3}H]G3139, and at various times after injection of G3139, plasma was collected and extracted for analysis of G3139. The [^{3}H] recovery from the G3139 extracted from plasma was >90% and the levels of dissociated label in [^{3}H]G3139 was low (5%). After [^{3}H]G3139 was injected into mice, the percentage degraded was low over the time-course studied, ranging from 12% to 17% over the first 30 min after injection and decreasing to 5% after 4 h. These values were determined from radioactivity counts of SDS-PAGE bands of molecular weight <5 kDa (Fig. 3). At 4 h, the low levels of fragmented ODN may have been due to dissociation of [^{3}H] and/or distribution from the circulation.

In addition, whole plasma samples were analyzed for G3139-protein association. At 5 min after i.v. injection, the majority of plasma G3139 appeared in the free form (i.e., 65% not protein bound; Fig. 3). Furthermore, the

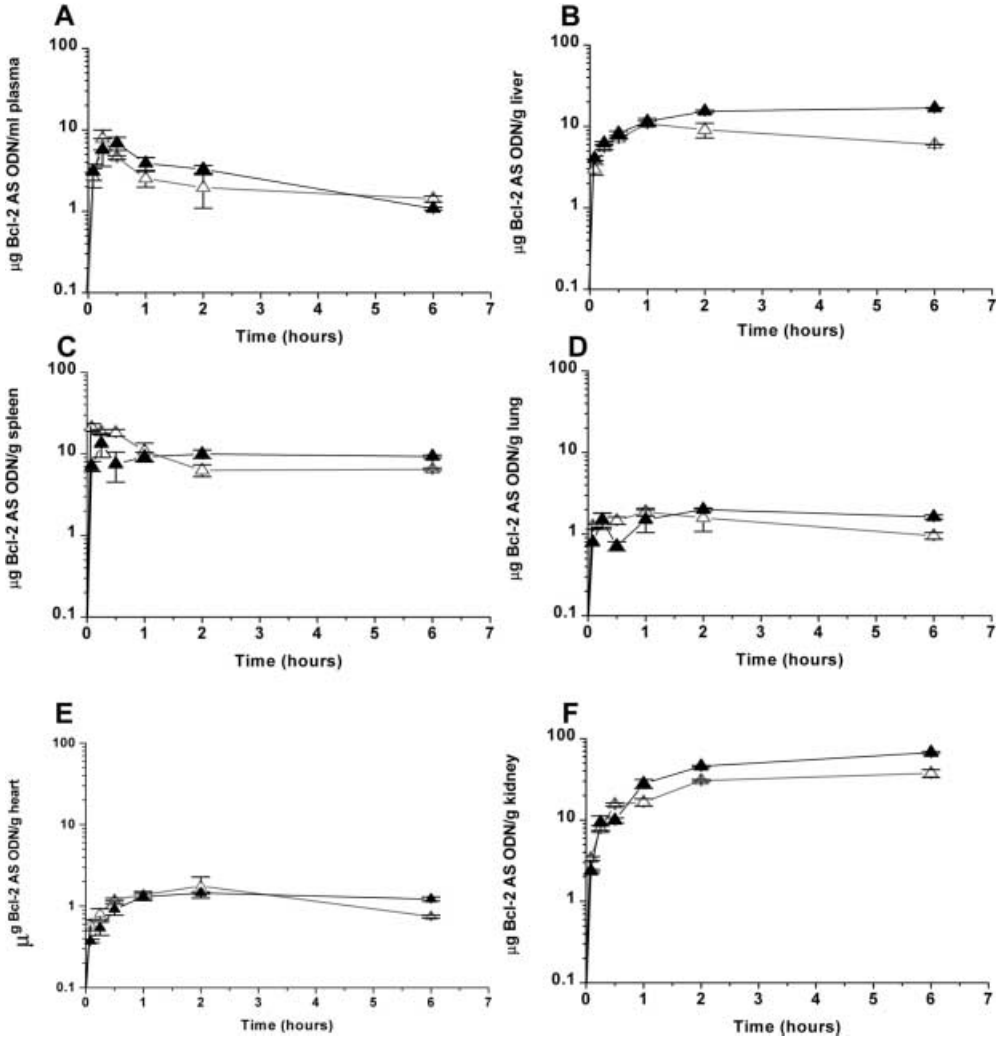

Fig. 2A–F Distribution profile of G3139 in plasma and various organs in MDA435/LCC6 tumor-bearing SCID-RAG2 mice after multiple treatments with G3139. Mice with tumors (0.1–0.15 g, day 17) were either injected with a single i.p. dose of [^{3}H]G3139 (5 mg/kg) (*open triangles*) or given three doses of G3139 (5 mg/kg) on days 17–19 prior to determination of [^{3}H]G3139 PK (*closed triangles*). Levels of G3139 in plasma (**A**), liver (**B**), spleen (**C**), lung (**D**), heart (**E**), and kidney (**F**) were determined at the indicated times using scintillation counting for [^{3}H] (see Materials and methods). Data are expressed as means ± SD ($n = 3$ mice per time-point)

association of G3139 with plasma proteins increased as a function of time (22% at 5 min to 50% at 4 h; Fig. 3), also seen as a reduction in the levels of free G3139 in plasma. The protein-associated forms of G3139 interacted with 20–50 kDa and ≥160 kDa proteins (Fig. 3), which may have been responsible for the slow elimination of G3139 from plasma.

Effect of coadministered DOX on the PK of G3139

When DOX was coadministered i.v. with i.p. G3139, subtle changes in the plasma PK of G3139 were observed (Table 1). An elevated G3139 Cmax was obtained in the presence of DOX (11.2 μg/ml compared to 6.9 μg/ml without DOX, $P < 0.05$). The absorption rate of G3139 from the i.p. cavity into plasma was enhanced fourfold in the presence of DOX with an increase in the K01 rate constant to 19.7 h^{-1} from 4.1 h^{-1} in the absence of DOX. In the presence of DOX, the volume of distribution increased to 7.7 ml (compared to 7.1 ml without DOX). Although the presence of DOX had a substantial effect on the $t_{1/2}\alpha$ (0.8 h vs 0.2 h, G3139 with and without DOX, respectively), the mean AUCs were not significantly different (19.7 μg·h/ml in the presence of DOX vs 17.4 μg·h/ml without DOX; $P > 0.05$). There were no substantial differences in the organ distribution of G3139 in the presence and absence of DOX (Fig. 4), although the splenic accumulation of G3139 in the presence of DOX appeared to be enhanced 1.5-fold after 2 h (Fig. 4C).

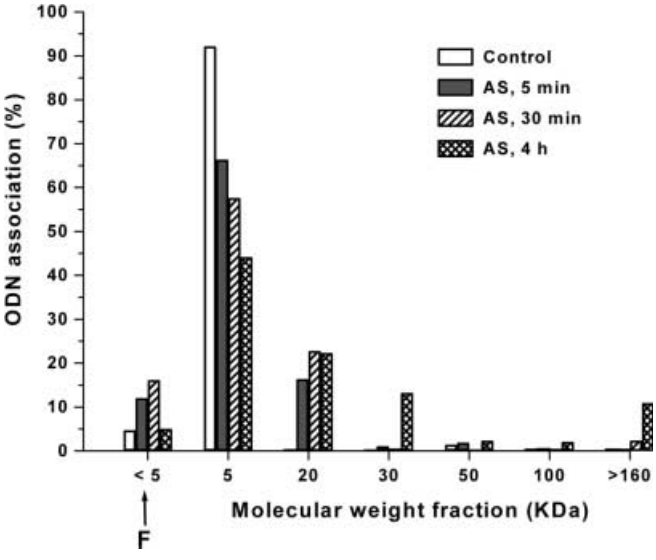

Fig. 3 SDS-PAGE molecular weight analysis of G3139 in plasma following i.v. injection of G3139 to SCID-RAG2 mice. Mice were injected with a single i.v. bolus of [^{3}H]G3139 (5 mg/kg) and plasma samples were collected at 5 min, 30 min and 4 h after G3139 injection. Isolated ODNs (see Methods) and plasma were run on a SDS-PAGE gel (12.5% and 20%). Intact ODN were those of 5 kDa molecular weight, fragmented ODN (*F*) were < 5 kDa and those associated with plasma components were > 5 kDa

We also evaluated the plasma levels of DOX in the presence and absence of G3139 to determine the relationship between G3139 PK and DOX PK (Fig. 5A, Table 1). Plasma DOX concentrations were largely unaltered in the presence of G3139 (Fig. 5A) and only subtle changes were observed in the descriptive PK properties compared to those with DOX alone (Table 1). The AUCs of DOX in the presence and absence of G3139 were not significantly different (3.2 μg·h/ml with G3139 treatment vs 3.0 μg·h/ml after DOX alone, $p > 0.05$). No metabolites of DOX (doxorubicinol and aglycone) were identified up to 2 h after injection. The levels of metabolites in plasma at 6 and 24 h were at low but non-quantifiable levels (< 10 ng/ml).

Tumor delivery of G3139

To evaluate the amount of G3139 reaching the tumor site, the [^{3}H] levels were determined as a function of time after i.v. or i.p. injection (Fig. 6A). We modeled the tumor data mathematically to a one-compartment model, to evaluate the descriptive tumor PK parameters and to elucidate the tumor microkinetics after various treatments (Table 2). G3139 following i.v. administration rapidly accumulated at the tumor site (Tmax 0.2 h) compared to accumulation following i.p. administration (Tmax 0.8 h), and the rate of absorption following i.v. administration (K01 56.9 h^{-1}) was approximately ninefold higher than following i.p. administration (K01 6.7 h^{-1}). Despite the higher plasma Cmax attained following i.v. than following i.p. administration (i.v. 99.9 μg/ml vs i.p. 8.6 μg/ml; Table 1), the peak tumor levels of G3139 attained with the two routes of administration (Cmax i.v. 5.2 μg/g tumor vs i.p. 5.7 μg/g tumor; $P > 0.05$) and the corresponding AUCs (i.v. 25.2 μg·h/g vs i.p. 22.6 μg·h/g; $P > 0.05$) were similar (Table 2). Unlike the muscle levels of G3139 (Fig. 6A, a vs b), the tumor G3139 uptake (tumor Cmax) appeared to be independent of plasma G3139 levels (or bioavailable dose) suggesting that G3139 uptake may be dependent upon certain inherent tumor pathology. Interestingly, G3139 demonstrated higher selectivity for tumor than for muscle tissue (Fig. 6A vs B), corresponding to a 2.5- to 3.8-fold higher tumor/muscle AUC ratio (Table 2). The concentration of G3139 was sustained at the tumor site for prolonged periods (Fig. 6A), corresponding to a low elimination rate constant K10 of 0.06 h^{-1} (Table 2).

Circulating levels of G3139 after three prior doses produced subtle effects on the tumor absorption profile of G3139. Administration of G3139 after three prior doses led to a decrease in absorption rate constant K01 (1.0 h^{-1}), an increase in K01 half-life (0.7 h) and an increase in Tmax (2.1 h) in tumor tissue compared to the values following a single i.p. dose of G3139 (Fig. 6B; Table 2). Despite the lower Cmax (4.9 μg/g tumor), the mean AUC (23.2 μg·h/g) was slightly higher, but this

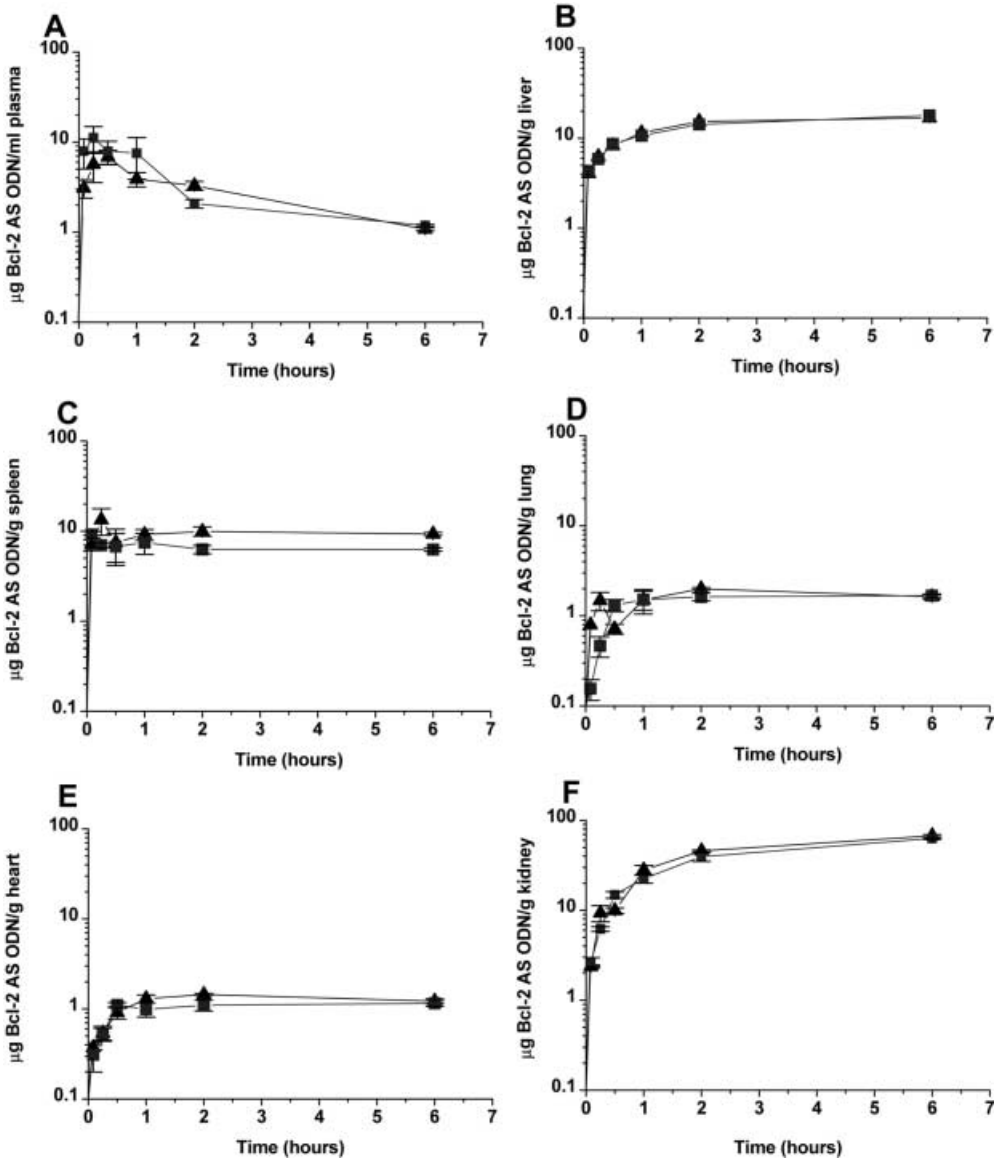

Fig. 4A–F Effect of doxorubicin (DOX) on the pharmacokinetics of G3139 in plasma and various organs in MDA435/LCC6 tumor-bearing SCID-RAG2 mice. Mice with tumors (0.1–0.15 g, day 17) were treated with G3139 (5 mg/kg) on days 17–19 and the PKs of G3139 were determined in the absence (*triangles*) and presence (*squares*) of DOX (5 mg/kg). Levels of G3139 in plasma (**A**), liver (**B**), spleen (**C**), lung (**D**), heart (**E**), and kidney (**F**) were determined at the indicated times using scintillation counting for [^{3}H] (see Materials and methods). Data are expressed as means ± SD ($n = 3$ mice per time-point)

was not significantly different from the values obtained with a single i.p. dose of G3139 ($P > 0.05$; Table 2). Also, no differences were seen in the tumor elimination rate constants (K10 0.15 h^{-1}), indicating that tumor retention was independent of circulatory G3139 concentration or prior G3139.

In the presence of DOX, relatively small differences were observed in the tumor accumulation rate of G3139 (Fig. 6C; Table 2). Interestingly, lower levels of G3139 were observed in tumors in the presence of DOX, corresponding to lower Cmax (3.7 μg/g tumor vs 4.9 μg/g tumor in the absence of DOX, $P < 0.05$) and AUC values (17.1 μg·h/g tumor vs 23.2 μg·h/g tumor without DOX, $P < 0.05$). In parallel experiments, the tumor DOX profiles were also examined to help elucidate the effect of G3139 on tumor DOX uptake (Fig. 5B; Table 2). Tumor DOX levels were markedly elevated in the presence of G3139 (Cmax 43.7 μg/g tumor) compared to the levels with DOX alone (Cmax 27.8 μg/g tumor, $P < 0.05$; Fig. 5B). The corresponding DOX AUCs were also significantly higher (696 and 480 μg·h/g tumor in the presence and absence of G3139, respectively, $P < 0.01$). The microkinetics of tumor DOX in the presence of G3139 were also substantially different (Table 2). There appeared to be a net transfer of DOX into tumors in the presence of G3139, seen as a sevenfold higher K01 (35 h^{-1}) compared to the transfer with DOX alone (K01 5 h^{-1}). However, this occurred with a twofold higher elimination rate constant in the presence of G3139 (K10 0.04 vs 0.02 h^{-1}). In addition, DOX metabolites were detected in tumors at low but non-quantifiable levels beyond 2 h after administration. Taken together, these results suggest possible G3139-DOX interactions at the tumor site, leading to preferential accumulation of DOX within tumors.

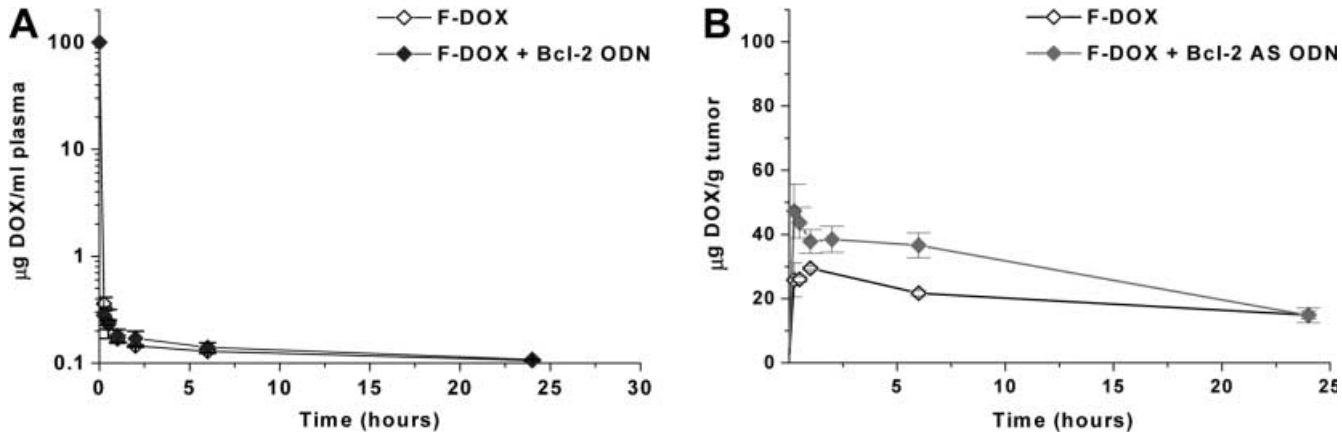

Fig. 5A, B Doxorubicin concentration-time profiles in plasma and tumor in the presence and absence of G3139 in MDA435/LCC6 tumor-bearing SCID-RAG2 mice. Mice with tumors (0.1–0.15 g) were injected with G3139 (5 mg/kg) daily on days 1–4. DOX was administered at 5 mg/kg on day 4, either in the presence (*closed diamonds*) or absence (*open diamonds*) of Bcl-2 AS G3139. Plasma samples (**A**) and tumor samples (**B**) were taken at the indicated times, and analyzed for DOX using HPLC. Data are expressed as means ± SD ($n = 3$ mice per time-point)

Discussion

The regulation of apoptosis or programmed cell death is under the control of several gene products and cross-talk between various intracellular signaling pathways [11]. In recent years, several attempts to achieve proapoptotic stimulation in tumor cells have targeted a family of proto-oncogenes, particularly Bcl-2 and homologues, Bcl-XL, Mcl-1, which have been implicated in the inhibition of apoptosis [24, 25, 26]. G3139, an AS phosphorothioate ODN to Bcl-2, has been shown to directly induce apoptosis [11] and several studies have shown that G3139 can act synergistically when combined with chemotherapeutics [12, 13, 14, 15, 16, 17, 18]. Clinical testing of G3139 has progressed to late phase II trials [27, 28], and combinations with mitoxantrone, docetaxel, Taxol, and dacarbazine are being explored [18, 29, 30, 31].

One issue regarding combining AS ODN therapy with anticancer drugs for chemosensitization purposes that has not been previously addressed is potential PK, metabolic or tissue interactions between the ODN and the coadministered chemotherapeutic agent. This becomes important when administering drugs with narrow therapeutic indices, where alteration in plasma drug levels could produce unwanted drug toxicities and potentially compromise therapeutic activity. We undertook such investigations in order to help differentiate the AS- from the ODN-related PK effects in the therapeutic activity of G3139. We first compared the PK of G3139 after i.v and i.p. administration since these are the two routes of administration commonly utilized for preclinical studies. Following i.v. injection of G3139 to SCID mice, we observed a biexponential plasma concentration-time curve with a short α half-life of 0.03 h and a longer β half-life of 9.8 h. The rapid excretion and distribution of G3139 in vivo leads to low AUCs necessitating repeated drug dosage regimens to maintain steady-state G3139 levels in plasma.

By comparison, i.p. G3139 injection produced a prolonged plasma terminal elimination half life of 8.9 h consistent with other PK studies using phosphorothioate ODNs [23, 32, 33]. The relative bioavailability of i.p. G3139 administration was 84% compared to i.v. G3139, reflecting the lack of significant adsorption constraints with the i.p. route. Peak concentrations of G3139 in organs after i.v. injection were markedly higher compared to after i.p. administration (particularly, spleen, lung, heart and kidneys) indicating the potential for toxicities that could occur with higher bolus doses. The peak tumor levels and AUCs following administration by the two routes (i.v. vs. i.p.) were very similar, which confirms the selection of i.p. dosing for therapeutic studies aimed at optimizing prolonged down-regulation of Bcl-2 protein.

In our studies, investigation of the PK of G3139 was followed by determination of the radioactive counts of G3139 in plasma and biological tissues following administration. It is important to note that degradation of ODN mediated by nucleases in plasma and any dissociation of the radioactive label could have led to inaccuracy in the prediction of the G3139 PK properties, and consequently, we confirmed the integrity of the G3139 in plasma by evaluating the molecular weight identity of the AS ODN. Our studies revealed that G3139 remains largely intact, with $< 17\%$ of the label degraded in plasma after 30 min, confirming the resistance of phosphorothioate ODNs to nuclease digestion [9, 23, 32, 33]. The levels of degraded label after 4 h appeared to be slightly lower (5%) possibly because of time-dependent fragmentation of G3139 to smaller metabolites with subsequent dissociation of [^{3}H]. In view of these results, it appears that the use of radiolabeled G3139 provided plasma PK parameters representative of intact G3139. We cannot definitely confirm that similar relationships hold for tissue-associated G3139 due to the potential for degradation during homogenization and extraction. It may be reasonable to predict that G3139 radioactivity

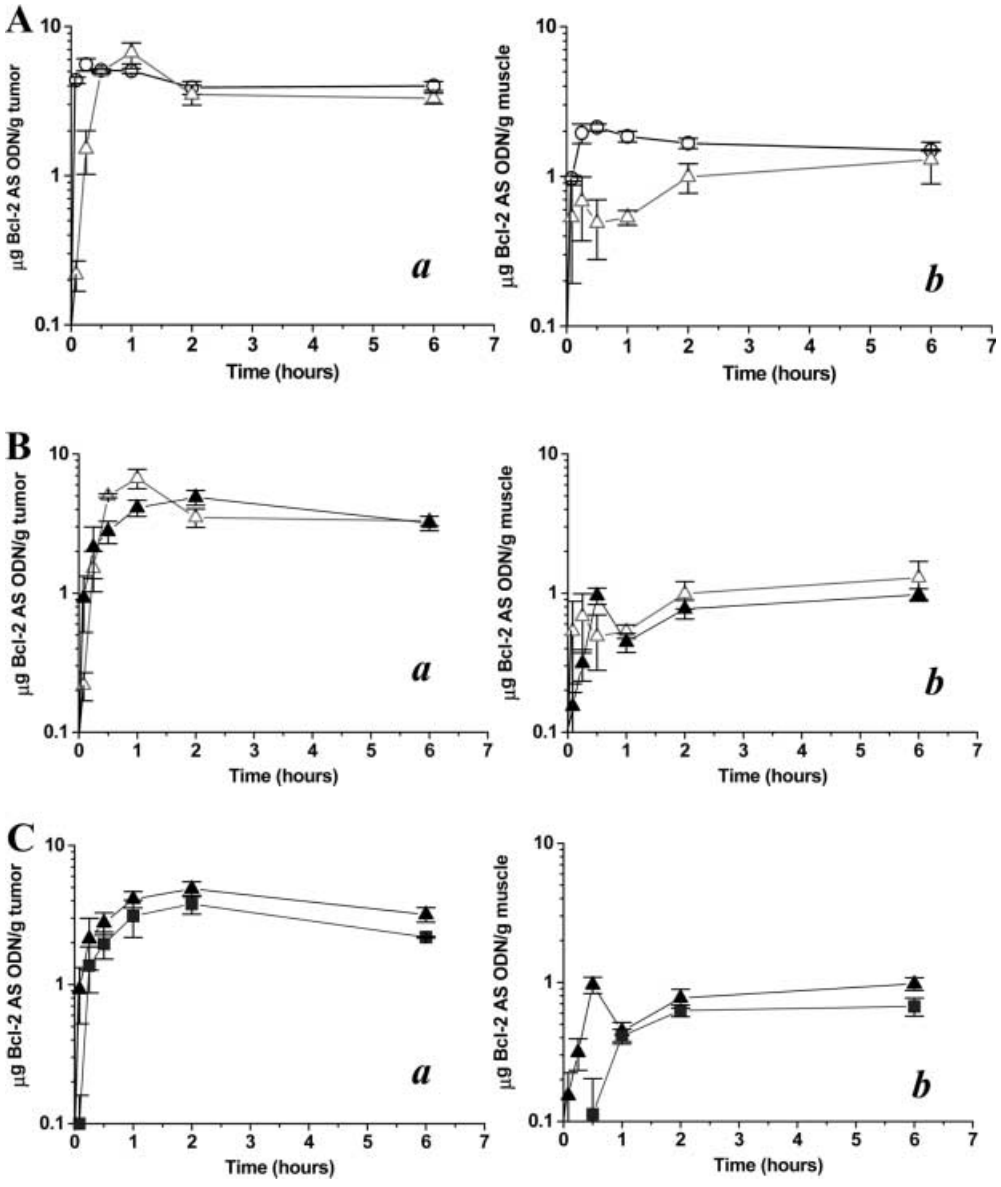

Fig. 6A–C Tumor and muscle accumulation profile of G3139 in MDA435/LCC6 tumor-bearing SCID-RAG2 mice. Mice with tumors (0.1–0.15 g, day 17) were injected with a single bolus dose of [^{3}H]G3139 (5 mg/kg) either i.v. (*open circles*) or i.p. (*open triangles*) (**A**), and the levels of G3139 determined in tumor (*a*) and muscle (*b*). Tumor (*a*) and muscle (*b*) pharmacokinetics of [^{3}H]G3139 were also determined after three doses of G3139 (5 mg/kg) on days 17–19 in the absence (*closed triangles*) (**B**) and presence (*closed squares*) (**C**) of DOX. Data are expressed as means ± SD ($n = 3$ mice per time-point)

levels in tissues with relatively low metabolic activity (e.g. muscle and tumor) are primarily intact G3139. Therefore, we believe that [^{3}H]G3139 can be used to identify important PK parameters for comparisons between different dosing regimens and combination treatments.

Since ODNs often need to be administered chronically to attain persistent modulation of target gene expression, we examined the PK effects of G3139 after repeated administration. Substantial changes were observed in the absorption and distribution rates of G3139 in vivo resulting from the presence of close to equilibrium levels in tissue compartments. Multiple treatments with G3139 were able to produce elevated and prolonged G3139 levels in tissues, increasing exposure of tumor cells to G3139. Extrapolation of these results to drug efficacy studies in MDA435/LCC6 tumors with such regimens of Bcl-2 AS ODNs in preclinical therapeutic models has indicated that sustained Bcl-2 levels in tumors correlate with downregulation of Bcl-2 protein and a reduction in tumor growth [16].

Combining DOX with G3139 produced subtle changes in the plasma G3139 PKs. Elevated plasma Cmax, AUC, and volume of distribution values of G3139 in the presence of DOX were possibly a result of G3139-DOX interactions in plasma. In parallel experiments, we also examined the effect of coadministered G3139 on DOX PKs. Interestingly, the plasma DOX PKs were relatively unaltered in the presence of G3139 in plasma. Changes in plasma G3139 PKs, but no substantial changes in the organ distribution of G3139, were observed in the presence of DOX. This could have been a result of direct G3139-DOX interactions in plasma in either free or protein-bound form, which may affect the excretory pathway of G3139. Further studies focusing specifically on metabolism and excretion properties of G3139 are required to fully elucidate these interactions.

Table 2 Summary of selected pharmacokinetic parameters of G3139 in tumor after the indicated treatments. RAG2 mice bearing MDA435/LCC6 tumors were treated with a single i.v. or i.p. dose of 5 mg/kg of G3139 on day 17 after tumor implantation when tumors weighed approximately 0.1 g. Mice were killed at selected times after [^{3}H]G3139 treatment and the amount of [^{3}H]G3139 in plasma determined using scintillation counting and DOX determined using a HPLC assay (see methods). Data are means ($n = 3$ mice per time-point, 18 mice per treatment group). PK parameters were estimated using WinNonLin using a one-compartment model with first order input and elimination (*Cmax* maximum concentration in tumor; *Tmax* time to Cmax; $AUC_{0\text{-}t}$ area under the concentration-time curve; *Vt* tumor volume of distribution; *K01*, *K10* absorption and elimination rate constants; *K01 half life*, *K10 half life* absorption and elimination half lives)

Drug	Route/ treatment	Cmax (μg/g tumor)	Tmax (h)	$AUC_{0\text{-}t}$ (μg·h/ml)	Vt (ml)	K01 half-life (h)	K10 half-life (h)	K01 (h^{-1})	K10 (h^{-1})	Tumor/muscle $AUC_{0\text{-}t}$
G3139	i.v.	5.2 ± 0.8	0.2	25.2 ± 2.6	19.2	0.01	12.22	56.9	0.06	2.5
	i.p.	5.7 ± 1.0	0.8	22.6 ± 2.3	16.3	0.10	5.07	6.7	0.14	3.8
	i.p. (after three prior i.p. doses)[a]	4.9 ± 0.7	2.1	23.2 ± 3.0	14.9	0.67	4.72	1.03	0.15	4.9
	i.p. (after three prior i.p. doses + DOX)[b]	3.7 ± 0.8	1.9	17.1 ± 1.9	19.7	0.56	4.21	1.24	0.16	5.4
DOX	i.v.	27.8 ± 3.8	1.0	480.9 ± 32.0	3.5	0.13	25.40	5.36	0.02	–
	i.v. (after three prior i.p. G3139 doses)[c]	43.7 ± 6.2	0.2	696.1 ± 63.5	2.3	0.02	15.87	35.37	0.04	–

[a]Mice were given 5 mg/kg of G3139 on days 17–19 and the G3139 PK determined on day 20
[b]Mice were given 5 mg/kg of G3139 on days 17–19 and the G3139 PK determined on day 20 in the presence of DOX (5 mg/kg given i.v. 1 h prior to G3139)
[c]Mice were given 5 mg/kg of G3139 on days 17–19 and the DOX PK determined on day 20

To date there have been no published reports on the kinetics of ODN transport into tumors in vivo. We observed a selective delivery of G3139 to tumor compared to muscle. We also demonstrated that high tumor levels of G3139 of approximately 4–6 μg/g tumor could be attained with i.p. administration, corresponding to approximately 3% of the injected dose. The mechanisms of ODN delivery to tumor cells remains largely unknown, although it has been speculated that protein-mediated transport may be involved. G3139 appears to interact with two specific molecular weight protein groups, i.e., 15–40 kDa and >160 kDa. The fact that a large fraction of the G3139 remained largely intact and in the free form indicates that free ODN passively accumulates in tumors. Our results indicate that a part of the G3139 remained protein bound, and the observed concentrations of G3139 in plasma may have been due to the circulating levels of the protein-bound form, possibly due to the high-affinity interactions of phosphorothioate ODNs with lipoproteins, heparin-binding proteins, albumin and/or α2 macroglobulins [34, 35, 36]. The exact mechanism of tumor AS ODN uptake and whether this occurs via the free or protein-associated form is still unclear. The fact that downregulation of the target protein can be achieved in vivo in this tumor model indicates that AS ODNs are released into the cytoplasm either via direct membrane-receptor trafficking or via the endosomal/lysosomal apparatus to allow hybridization with the target Bcl-2 mRNA [16]. Based on our tumor uptake of 5 μg/g tumor weight, we estimated the G3139 uptake to be 400,000 molecules available/tumor cell (from a G3139 molecular weight of 5685 g/mole, and assuming a homogeneous population of 10^9 tumor cells/g tumor).

In tumor tissue, in the presence of coadministered DOX, very subtle changes were observed in the G3139 accumulation rate, corresponding to a slightly lower Cmax and AUC of G3139. More striking, however, was our observation that tumor exposure to DOX was increased by the presence of coadministered G3139 and that this was achieved in the absence of plasma DOX PK alterations. The PK interactions between G3139 and DOX appear to favor selective delivery to tumor tissue. The plasma exposure to DOX in mice treated with G3139 was minimally reduced compared to no G3139 treatment whereas tumor exposure to DOX was increased two- to threefold. The reasons for these changes are not fully understood, but could be related to enhanced drug permeability of tumor tissue treated with G3139. The increased tumor uptake of DOX-G3139 complexes from the circulation and increased binding of DOX to tumor cells could arise from altered permeability of these complexes at the tumor site. We have shown that treatment of MDA435/LCC6 tumors with G3139 results in significant apoptosis [16]. Alternatively, due to the high DNA binding capacity of DOX, this could permit elevated drug levels at the tumor site due to DOX intercalation with exposed DNA in tumor cells undergoing apoptosis. The presence of DOX at the tumor site may depend upon the dissociation of the DOX-ODN complex, release of DOX from cellular DNA, or removal by macrophages that are involved in engulfment of cells undergoing apoptosis (in this case with G3139 and DOX).

In summary, we showed that analysis of radiolabeled G3139 PK parameters provides useful information that could help establish optimized treatment regimens and correlate the PK information with tumor delivery and therapeutic activity in preclinical tumor models. As such pharmacodynamic relationships are established, we could then predict the potential impact of specific treatment combinations on antitumor activity. In the

case of DOX, such interactions appear favorable in that elevated tumor drug levels were achieved without compromising G3139 tumor uptake. This type of information may be very useful when designing treatment protocols combining ODNs and other anticancer drugs.

Acknowledgements The authors wish to thank Rebecca Ng for her excellent technical assistance. This work was supported by a grant from the National Cancer Institute of Canada (NCIC) with funds from the Canadian Cancer Society. Daniel Lopes de Menezes is a Terry Fox Research Fellow of the NCIC, supported with funds from the CURE Foundation for Cancer Research.

References

1. Reed JC, Miyashita T, Takayama S, Wang HG, Sato T (1996) Bcl-2 family proteins: regulators of cell death involved in the pathogenesis of cancer and resistance to therapy. J Cell Biochem 60:23
2. Kamesaki S, Kamesaki H, Jorgensen TJ, Tanizawa A, Pommier Y, Cossman J (1993) Bcl-2 protein inhibits etoposide-induced apoptosis through its effects on events subsequent to topoisomerase II-induced DNA strand breaks and their repair. Cancer Res 53:4251
3. Miyashita T, Reed JC (1993) Bcl-2 oncoprotein blocks chemotherapy-induced apoptosis in a human leukemia cell line. Blood 81:151
4. Walton MI, Whysong D, O'Connor PM, Hockenbery D, Korsmeyer SJ, Kohn KW (1993) Constitutive expression of human Bcl-2 modulates nitrogen mustard and camptothecin induced apoptosis. Cancer Res 53:1853
5. Cotter FE, Johnson P, Hall P, Pocock C, Al Mahdi N, Cowell JK, Morgan G (1994) Antisense oligonucleotides suppress B-cell lymphoma growth in a SCID-hu mouse model. Oncogene 9:3049
6. Reed JC, Stein C, Subasinghe C, Haldar S, Croce CM, Yum S, Cohen J (1990) Antisense-mediated inhibition of BCL2 protooncogene expression and leukemic cell growth and survival: comparisons of phosphodiester and phosphorothioate oligodeoxynucleotides. Cancer Res 50:6565
7. Zamecnik PC, Stephenson ML (1978) Inhibition of Rous sarcoma virus replication and cell transformation by a oligodeoxynucleotide. Proc Natl Acad Sci U S A 75:280
8. Agrawal S (1999) Importance of nucleotide sequence and chemical modifications of antisense oligonucleotides. Biochim Biophys Acta 1489:53
9. Raynaud FI, Orr RM, Goddard PM, Lacey HA, Lancashire H, Judson IR, Beck T, Bryan B, Cotter F (1997) Pharmacokinetics of G3139, a phosphorothioate oligodeoxynucleotide antisense to bcl-2, after intravenous administration or continuous subcutaneous infusion to mice. J Pharmacol Exp Ther 281:420
10. Reed JC (1999) Mechanisms of apoptosis avoidance in cancer. Curr Opin Oncol 11:68
11. Webb SJ, Harrison DJ, Wylie AH (1997) Apoptosis: an overview of the process and its relevance in disease. In: Kaufmann S (ed) Apoptosis, pharmacological implications and therapeutic opportunities (Advances in pharmacology). Academic Press, New York, p 1
12. Jansen B, Schlagbauer-Wadl H, Brown BD, Bryan RN, van Elsas A, Muller M, Wolff K, Eichler H, Pehamberger H (1998) Bcl-2 antisense therapy chemosensitizes human melanoma in SCID mice. Nat Med 4:232
13. Zangemeister-Witte U, Schenker T, Luedke GH, Stahel RA (1998) Synergistic cytotoxicity of Bcl-2 antisense oligodeoxynucleotide and etoposide, doxorubicin and cisplatin in small-cell lung cancer cell lines. Br J Cancer 78:1035
14. Konopleva M, Tari AM, Estrov Z, Harris D, Xie Z, Zhao S, Lopez-Berestein G, Andreeff M (2000) Liposomal Bcl-2 antisense oligonucleotides enhance proliferation, sensitize acute myeloid leukemia to cytosine-arabinoside, and induce apoptosis independent of other antiapoptotic proteins. Blood 95:3929
15. Leung S, Miyake H, Zellweger T, Tolcher A, Gleave ME (2001) Synergistic chemosensitization and inhibition of progression to androgen independence by antisense Bcl-2 oligodeoxynucleotide and paclitaxel in the LNCaP prostate tumor model. Int J Cancer 91:846
16. Lopes de Menezes DE, Hudon N, McIntosh N, Mayer LD (2000) Therapeutic and pharmacokinetic properties of free and liposomal doxorubicin combined with Bcl-2 antisense oligonucleotide treatment. Clin Cancer Res 6:2891
17. Klasa RJ, Bally MB, Ng R, Goldie JH, Gascoyne R, Wong FMP (2000) Eradication of human non-Hodgkin's lymphoma in SCID mice by Bcl-2 antisense oligonucleotides combined with low dose cyclophosphamide. Clin Cancer Res 6:2492
18. Jansen B, Wacheck V, Heere-Ress E, Schlagbauer-Wadl H, Hoeller C, Lucas T, Hoermann M, Hollenstein U, Wolff K, Pehamberger H (2000) Chemosensitisation of malignant melanoma by BCL2 antisense therapy. Lancet 356:1728
19. Waters JS, Webb A, Cunningham D, Clarke PA, Raynaud F, di Stefano F, Cotter FE (2000) Phase I clinical and pharmacokinetic study of bcl-2 antisense oligonucleotide therapy in patients with non-Hodgkin's lymphoma. J Clin Oncol 18:1812
20. Leonessa F, Green D, Licht T, Wright A, Wingate-Legette K, Lippman J, Gottesman MM, Clarke R (1996) MDA435/LCC6 and MDA435/LCC6MDR1: ascites models of human breast cancer. Br J Cancer 73:154
21. Mayer LD, Tai LCL, Ko DSC, Masin D, Ginsberg RS, Cullis PR, Bally MB (1989) Influence of vesicle size, lipid composition, and drug-to-lipid ratio on the biological activity of liposomal doxorubicin in mice. Cancer Res 49:5922
22. Krishna R, Mayer LD (1997) Liposomal doxorubicin circumvents PSC833-free drug interactions, resulting in effective therapy of multidrug-resistant solid tumors. Cancer Res 57:5246
23. Agrawal S, Temsamani J, Tang JY (1991) Pharmacokinetics, biodistribution, and stability of oligodeoxynucleotide phosphorothioates in mice. Proc Natl Acad Sci U S A 88:7595
24. Reed JC (1997) Bcl-2 family proteins: regulators of apoptosis and chemoresistance in hematologic malignancies. Semin Hematol 34:9
25. Lebedeva I, Rando R, Ojwang J, Cossum P, Stein CA (2000) Bcl-xL in prostate cancer cells: effects of overexpression and down-regulation on chemosensitivity. Cancer Res 60:6052
26. Moulding DA, Giles RV, Spiller DG, White MR, Tidd DM, Edwards SW (2000) Apoptosis is rapidly triggered by antisense depletion of MCL-1 in differentiating U937 cells. Blood 96:1756
27. Dean NM, Griffey RH (1997) Identification and characterization of second-generation antisense oligonucleotides. Antisense Nucleic Acid Drug Dev 7:229
28. Webb A, Cunningham D, Cotter F, Clarke PA, di Stefano F, Ross P, Corbo M, Dziewanowska Z (1997) Bcl-2 antisense therapy in patients with non-Hodgkin lymphoma. Lancet 349:1137
29. Chi KN, Gleave ME, Klasa R, Murray N, Bryce C, Tolcher A (2000) A phase I trial of an antisense oligonucleotide to Bcl-2 (G3139, Genta) and mitoxantrone in patients with metastatic hormone refractory prostate cancer (HRPC). Proc Am Soc Clin Oncol 19:330
30. Chen HX, Marshall JL, Trocky N, Ling Y, Baidas S, Rizvi N, Bhargava P, Lippman ME, Yang D, Hayes DF (2000) A phase I study of Bcl-2 antisense G3139 (Genta) and weekly docetaxel in patients with advanced breast cancer and other solid tumors. Proc Am Soc Clin Oncol 19:178
31. Scher HI, Morris MJ, Tong WP, Cordon-Cardo C, Drobnjak M, Kelly WK, Slovin SF, Terry KL, DiPaola RS, Rafi M, Rosen N (2000) A phase I trial of G3139 (Genta Inc.) a Bcl-2 antisense drug, by continuous infusion (CI) as a single agent and with weekly Taxol (T). Proc Am Soc Clin Oncol 19:199
32. DeLong RK, Nolting A, Fisher M, Chen Q, Wickstrom E, Kligshteyn M, Demirdji S, Caruthers M, Juliano RL (1997) Comparative pharmacokinetics, tissue distribution, and tumor

accumulation of phosphorothioate, phosphorodithioate, and methylphosphonate oligonucleotides in nude mice. Antisense Nucleic Acid Drug Dev 7:71
33. Sands H, Gorey-Feret LJ, Cocuzza AJ, Hobbs FW, Chidester D, Trainor GL (1994) Biodistribution and metabolism of internally ^{3}H-labeled oligonucleotides. I. Comparison of a phosphodiester and a phosphorothioate. Mol Pharmacol 45:932
34. McCormack JJ, Bigelow JC, Chrin LR, Mathews LA (1990) High performance liquid chromatographic analysis of phosphorothioates in biological fluids. J Chromatogr 533:133
35. Zhang X, Lu Z, Diasio RB, Jiang Z, Tan W, Agrawal S, Zhang R (1995) Plasma and serum protein binding of antisense oligodeoxynucleotide phosphorothioates in experimental animals and humans. Proc Am Assoc Cancer Res 36:411
36. de Smidt PC, Le Doan T, de Falco S, van Berkel TJ (1991) Association of antisense oligonucleotides with lipoproteins prolongs the plasma half-life and modifies the tissue distribution. Nucleic Acids Res 19:4695